Lattice calculation of the strangeness magnetic moment of the nucleon

S. J. Dong and K. F. Liu

Department of Physics and Astronomy, University of Kentucky, Lexington, Kentucky 40506

A. G. Williams

Special Research Center for the Subatomic Structure of Matter and Department of Physics and Mathematical Physics,
University of Adelaide, 5005 Australia

We report on a lattice QCD calculation of the strangeness magnetic moment of the nucleon. Our result is $G_M^s(0) = -0.36 \pm 0.20$. The sea contributions from the u and d quarks are about 80% larger. However, they cancel to a large extent due to their electric charges, resulting in a smaller net sea contribution of $-0.097 \pm 0.037 \mu_N$ to the nucleon magnetic moment. As far as the neutron to proton magnetic moment ratio is concerned, this sea contribution tends to cancel out the cloud-quark effect from the Z graphs and results in a ratio of -0.68 ± 0.04 which is close to the SU(6) relation and the experiment. The strangeness Sachs electric mean-square radius $\langle r_s^2 \rangle_E$ is found to be small and negative. [S0556-2821(98)01817-7]

PACS number(s): 13.40.Em, 12.38.Gc, 14.20.Dh

The strangeness content of the nucleon has been a topic of considerable recent interest for a variety of reasons. The studies of nucleon spin structure functions in polarized deep inelastic scattering experiments at CERN and SLAC [1], combined with neutron and hyperon β decays, have turned up a surprisingly large and negative polarization from the strange quark. In addition, there is a well-known long-standing discrepancy between the pion-nucleon sigma term extracted from the low energy pion-nucleon scattering [2] and that from the octect baryon masses [3]. This discrepancy can be reconciled if a significant $\bar{s}s$ content in the nucleon [4,3] is admitted.

This naturally leads to the question as to how important the strange quarks are in the vector, pseudoscalar, and tensor matrix elements. The case of the vector current matrix element $\langle N|\bar{s}\gamma_\mu s|N\rangle$ is especially interesting. If the strange magnetic moment (MM) is large, it is likely to spoil the nice SU(6) prediction of the neutron to proton MM ratio of $-2/3$ which lends credence to the valence quark picture. On the other hand, if it is small one would like to understand why it should be different from the axial-vector and scalar cases.

To address some of these issues, an experiment to measure the neutral weak magnetic form factor G_M^Z via elastic parity-violating electron scattering was recently carried out by the SAMPLE Collaboration [5]. The strangeness magnetic form factor is obtained by subtracting out the nucleon magnetic form factors G_M^p and G_M^n. The reported value is $G_M^s(Q^2 = 0.1 \text{ GeV}^2) = +0.23 \pm 0.37 \pm 0.15 \pm 0.19$. Future experiments have the promise of tightening the errors and isolating the radiative corrections so that we can hope to have a well-determined value and sign for $G_M^s(0)$.

Theoretical predictions of $G_M^s(0)$ vary widely. The values from various models and analyses range from -0.75 ± 0.30 in a QCD equalities analysis [6] to $+0.37$ in an SU(3) chiral bag model [7]. While a few give positive values [7,8], most model predictions are negative with a typical range of -0.25 to -0.45 [6,9–14]. Summaries of these predictions can be found in Refs. [6,14]. A similar situation exists for the strangeness electric mean-square radius $\langle r_s^2 \rangle_E$. A number of the predictions are positive [9,13], while the others are negative [8,10–12,14]. Elastic $\vec{e}p$ and $\vec{e}^4$He parity-violation experiments are currently planned at TJNAF [15] to measure the asymmetry A_{LR} at forward angles to extract $\langle r_s^2 \rangle_E$. Hopefully, they will settle the issue of its sign.

In view of the large spread of theoretical predictions for both $G_M^s(0)$ and $\langle r_s^2 \rangle_E$ and in view of the fact that the experimental errors on $G_M^s(0)$ are still large, it is clearly important to perform a first-principle lattice QCD calculation in the hope that it will shed some light on these quantities. Our previous results on flavor-singlet quantities which involve the so-called "disconnected insertions" (DI) for the sea quarks in addition to the "connected insertions" (CI) for the valence and cloud quarks [16,17] reveal that the sea quark contribution to the flavor-singlet g_A^0 from the DI is negative and the magnitude large enough (e.g., the strangeness polarization $\Delta s = 0.12 \pm 0.01$) to cancel the positive CI contribution to a large extent. This results in a small g_A^0 at 0.25 ± 0.12, which is in agreement with the experimental results [1]. Similarly, the calculated ratio $y = \langle N|\bar{s}s|N\rangle / \langle N|\bar{u}u + \bar{d}d|N\rangle = 0.36 \pm 0.03$ [16,17] gives the right amount of strangeness content to resolve the $\pi N \sigma$ puzzle we alluded to earlier. Given these reasonably successful estimates of strangeness in the axial-vector and scalar channels, we feel that it should yield meaningful results in the vector current as well. In particular, we would like to understand why the SU(6) valence quark picture fails badly in the flavor-singlet axial-vector and scalar cases and yet gives an apparently good prediction in the neutron to proton MM ratio—a yet unresolved puzzle in low-energy hadron physics.

The lattice formulation of the electromagnetic form factors has been given in detail in the past [18]. Here, we shall concentrate on the DI contribution, where the strangeness current contributes. In the Euclidean formulation, the Sachs EM form factors can be obtained by the combination of two- and three-point functions

$$G_{NN}^{\alpha\alpha}(t,\vec{p}) = \sum_{\vec{x}} e^{-i\vec{p}\cdot\vec{x}} \langle 0|\chi^{\alpha}(x)\bar{\chi}^{\alpha}(0)|0\rangle \quad (1)$$

$$G_{NV_{\mu}N}^{\alpha\beta}(t_f,\vec{p},t,\vec{q}) = \sum_{\vec{x}_f,\vec{x}} e^{-i\vec{p}\cdot\vec{x}_f+i\vec{q}\cdot\vec{x}}$$

$$\times \langle 0|\chi^{\alpha}(x_f)V_{\mu}(x)\bar{\chi}^{\beta}(0)|0\rangle, \quad (2)$$

where χ^{α} is the nucleon interpolating field and $V_{\mu}(x)$ the vector current. With large Euclidean time separation, i.e., $t_f - t \gg a$ and $t \gg a$, where a is the lattice spacing,

$$\frac{\Gamma_i^{\beta\alpha}G_{NV_jN}^{\alpha\beta}(t_f,\vec{0},t,\vec{q})}{G_{NN}^{\alpha\alpha}(t_f,\vec{0})} \frac{G_{NN}^{\alpha\alpha}(t,\vec{0})}{G_{NN}^{\alpha\alpha}(t,\vec{q})} \rightarrow \frac{\varepsilon_{ijk}q_k}{E_q+m}G_M(q^2), \quad (3)$$

$$\frac{\Gamma_E^{\beta\alpha}G_{NV_4N}^{\alpha\beta}(t_f,\vec{0},t,\vec{q})}{G_{NN}^{\alpha\alpha}(t_f,\vec{0})} \frac{G_{NN}^{\alpha\alpha}(t,\vec{0})}{G_{NN}^{\alpha\alpha}(t,\vec{q})} \rightarrow G_E(q^2), \quad (4)$$

where $\Gamma_i = \sigma_i(1+\gamma_4)/2$ and $\Gamma_E = (1+\gamma_4)/2$.

We shall use the conserved current from the Wilson action which, being point-split, yields slight variations on the above forms and these are given in Ref. [18]. Our 100 quenched gauge configurations were generated on a $16^3 \times 24$ lattice at $\beta = 6.0$. In the time direction, fixed boundary conditions were imposed on the quarks to provide larger time separations than available with periodic boundary conditions. We also averaged over the directions of equivalent lattice momenta in each configuration; this has the desirable effect of reducing error bars. Numerical details of this procedure are given in Refs. [18,19]. The dimensionless nucleon masses $M_N a$ for $\kappa = 0.154$, 0.152, and 0.148 are 0.738(16), 0.882(12), and 1.15(1) respectively. The corresponding dimensionless pion masses $m_\pi a$ are 0.376(6), 0.486(5), and 0.679(4). Extrapolating the nucleon and pion masses to the chiral limit we determine $\kappa_c = 0.1567(1)$ and $m_N a = 0.547(14)$. Using the nucleon mass to set the scale to study nucleon properties [19,16], the lattice spacing $a^{-1} = 1.72(4)$ GeV is determined. The three κ's then correspond to quark masses of about 120, 200, and 360 MeV respectively.

The strangeness current $\bar{s}\gamma_\mu s$ contribution appears in the DI only. In this case, we sum up the current insertion t from the nucleon source to the sink in Eqs. (3) and (4) to gain statistics [16]. This leads to const$+t_f G_{E,dis}(q^2)$ for Eq. (4). For Eq. (3), we average over the three spatial components $\bar{s}\gamma_i s$ and obtain const$+t_f[|\vec{q}|/(E_q+m)]G_{M,dis}(q^2)$. Similar to our studies of Δs and $\langle N|\bar{s}s|N\rangle$ [16], we use 300 complex Z_2 noises [20] and 100 gauge configurations to calculate the sea quark contribution (DI) with $\kappa = 0.148$, 0.152, and 0.154. In calculating the strange current, we have considered the correlation between the sea quark loop with $\kappa_s = 0.154$ and the valence quarks at $\kappa_v = 0.148$, 0.152, and 0.154. The ratio in Eq. (3) with the sum in t and average in V_i, which leads to the expression const$+t_f G_{M,dis}(q^2)$, is plotted in Fig. 1 as a function of t_f for $|\vec{q}| = 2\pi/La$. $G_{M,dis}(q^2)$ from the DI is obtained from fitting the slopes in the region $t_f \geq 8$ where
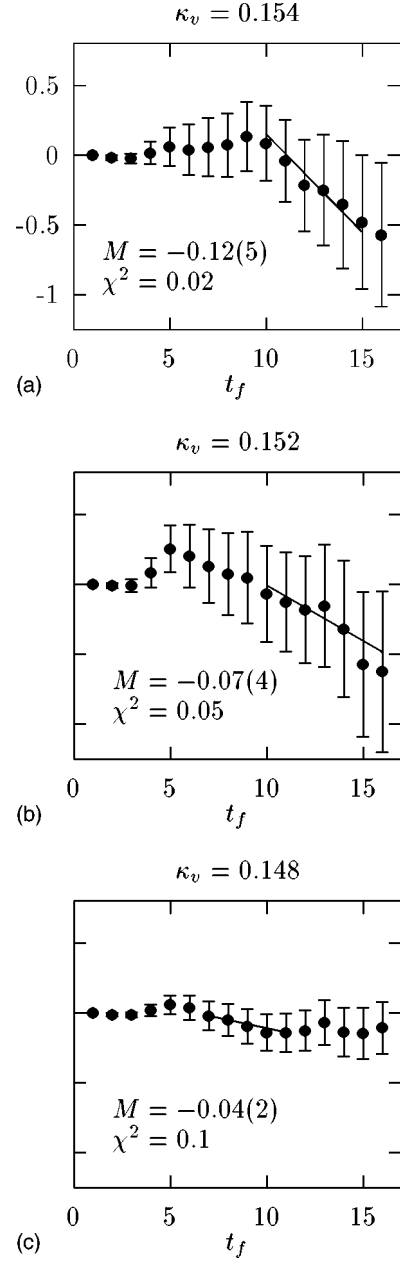

FIG. 1. The ratio of Eq. (3) as a function of t_f so that the slope is $G_{M,dis}(q^2)$ at $|\vec{q}| = 2\pi/La$. The sea quark is fixed at $\kappa_s = 0.154$ and the valence quark are at several κ_v. M is the fitted slope.

the nucleon is isolated from its excited states with the correlation among the time slices taken into account [16]. The resultant straight-line fits covering the ranges of t_f with the minimum χ^2 are plotted in Fig. 1. Finally, the errors on the fit, also shown in the figure, are obtained by jackknifing the procedure. To obtain the physical $G_M^s(q^2)$, we extrapolate the valence quarks to the chiral limit while keeping the sea quark at the strange quark mass (i.e., $\kappa_s = 0.154$). It has been shown in the chiral perturbation theory with a kaon loop that $G_M^s(0)$ is proportional to m_K, the kaon mass [21]. Thus, we extrapolate with the form $C + D\sqrt{\hat{m}+m_s}$ where $\hat{m}$ is the average u and d quark mass and m_s the strange quark mass to reflect the m_K dependence. This is the same form
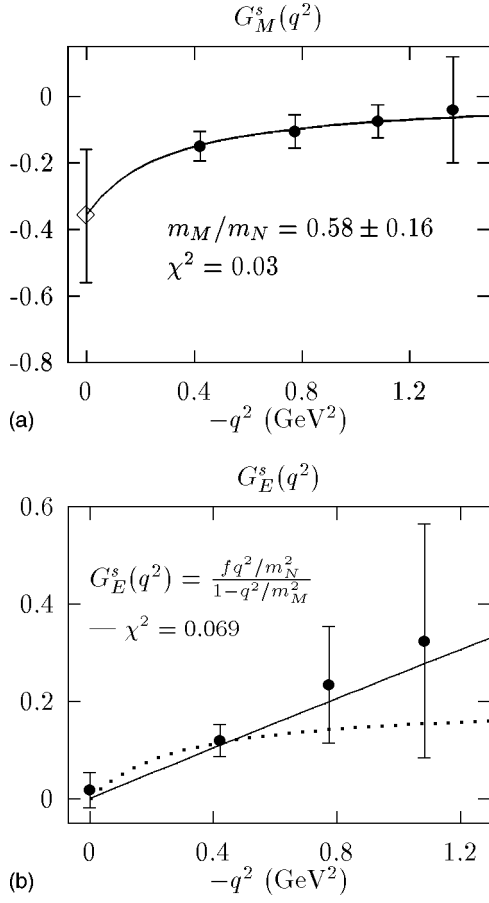
FIG. 2. (a) Strange magnetic form factor $G_M^s(q^2)$. $G_M^s(0)$ is indicated by $\diamond$. (b) Strangeness electric form factor $G_E^s(q^2)$. The solid line is a fit with the form shown in the figure and the dashed line is obtained with m_M from $G_M^s(q^2)$ in (a).

adopted for extracting $\langle N|\bar{s}s|N\rangle$ in Ref. [16], which also involves a kaon loop in the chiral perturbation theory.

Plotted in Fig. 2(a) is the extrapolated $G_M^s(q^2)$ at 4 non-zero q^2 values. The errors are again obtained by jackknifing the extrapolation procedure with the covariance matrix used to include the correlation among the three valence κ's. In view of the fact that the scalar current exhibits a very soft form factor for the sea quark [i.e., $g_{S,\text{dis}}(q^2)$] which has been fitted well with a monopole form [16], we shall similarly use
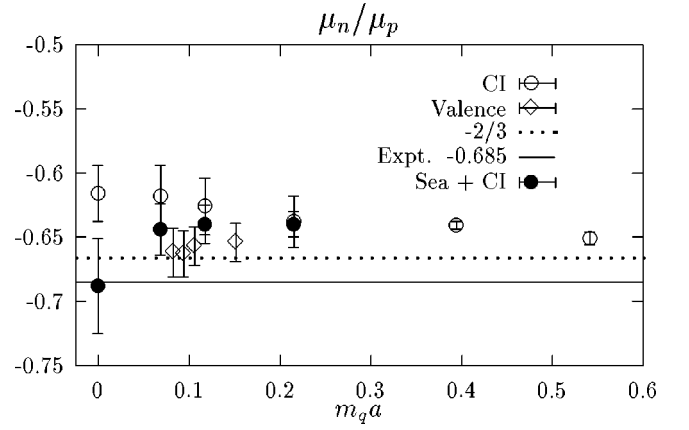

FIG. 3. Neutron to proton MM ratio μ_n/μ_p as a function of the dimensionless quark mass $m_q a$.

a monopole form to extrapolate $G_M^s(q^2)$ with nonzero q^2 to $G_M^s(0)$. Indicated as $\diamond$ in Fig. 2(a), $G_M^s(0)=-0.36\pm0.20$. Again, the correlation among the 4 q^2 are taken into account and the error is from jackknifing the fitting procedure. This is consistent with the recent experimental value within errors (see Table I). To explore the uncertainty of the q^2 dependence, we also fitted $G_M^s(q^2)$ with a dipole form and found $G_M^s(0)=-0.27\pm0.12$ with a dipole mass $m_D/m_N=1.19\pm0.22$. Similar results are obtained for u and d quarks with monopole fits. They turn out to be $G_{M,\text{dis}}^{u/d}(0)=-0.65\pm0.30$, which is about 1.8 times the size of $G_M^s(0)$.

Now, we are ready to address the question of why the SU(6) relation is badly broken in the scalar current (e.g., F_S, D_S) and axial current (e.g., g_A^0) and yet is so good for the neutron-proton magnetic moment ratio μ_n/μ_p. The lattice calculations for the scalar and axial currents [16] reveal the fact that the SU(6) breaking comes from both the sea quarks in the DI and the cloud quarks in the CI. We shall see how these degrees of freedom play out in the case of the MM. We first plot in Fig. 3 the ratio μ_n/μ_p for the CI part (shown as $\bigcirc$) as a function of the valence quark mass. We see that when the quark mass is in the charm region ($m_q a$ at 0.55 corresponds to $m_q\sim1$ GeV), the ratio is close to the SU(6) prediction of $-2/3$. This is quite reasonable as this is in the nonrelativistic regime where one expects SU(6) to work well. As the quark mass comes down to the strange region

TABLE I. Strangeness and proton-neutron MM and charge radii in comparison with experiments.

	Lattice	Experiments
$G_M^s(0)$	-0.36 ± 0.20	$G_M^s(Q^2=0.1\ \text{GeV}^2)=0.23\pm0.37\pm0.15\pm0.19$ [5]
$G_{M,\text{dis}}^u(0)$	-0.65 ± 0.30	
μ_{dis}	$-0.097\pm0.037\mu_N$	
μ_p	$2.62\pm0.07\mu_N$	$2.79\mu_N$
μ_n	$-1.81\pm0.07\mu_N$	$-1.91\mu_N$
μ_n/μ_p	-0.68 ± 0.04	-0.685
$\langle r_s^2\rangle_E$	$-0.061(3) - -0.16(6)\ \text{fm}^2$	
$\langle r^2\rangle_E^p$	$0.636\pm0.046\ \text{fm}^2$	$0.659\ \text{fm}^2$ [22]
$\langle r^2\rangle_E^n$	$-0.123\pm0.019\ \text{fm}^2$	$-0.127\ \text{fm}^2$ [22]

$(m_q a = 0.07)$, the ratio becomes less negative. Extrapolated to the chiral limit, the ratio is -0.616 ± 0.022 which deviates from the SU(6) prediction by 8%. We understand this deviation as mainly due to the cloud quark effect in the Z graphs. As we switch off these Z graphs in a valence approximation [16], the ratio (plotted as $\diamond$ in Fig. 3) becomes closer to the SU(6) value which resembles the nonrelativistic case. Similar behaviors were observed for the scalar and axial matrix elements [16]. Now we add the sea quark contribution from the DI to give $\mu_{\mathrm{dis}} = [2/3 G^u_{M,\mathrm{dis}}(0) - 1/3 G^d_{M,\mathrm{dis}}(0) - 1/3 G^s_M(0)] \mu_N$ to the CI and find that it tends to cancel the cloud effect and bring the ratio back to be similar to what the valence approximation predicts. For the $G^s_M(0)$ at various κ_v, we use the $G^s_M(0)/G^u_{M,\mathrm{dis}}(0)$ ratio from the chiral limit to obtain it from the $G^u_{M,\mathrm{dis}}(0)$ at each κ_v. At the chiral limit, when the total sea contribution $\mu_{dis} = -0.097 \pm 0.037 \mu_N$ is added to the CI, the μ_n/μ_p ratio then comes down to -0.68 ± 0.04 which is consistent with the experimental value of -0.685. We note that the μ_n/μ_p ratio for the full result ($\bullet$) is more negative at the chiral limit compared with those at other $m_q a$. This has to do with the fact that the CI employs the linear quark mass extrapolation, as do other observables for the CI [16,19], whereas the DI uses the $\sqrt{m_q}$ dependence for the chiral extrapolation as mentioned above. From this analysis, we see that although the individual $G^u_{M,\mathrm{dis}}(0), G^d_{M,\mathrm{dis}}(0)$, and $G^s_M(0)$ are large, their net contribution μ_{dis} is much smaller because of the partial cancellation due to the quark charges of u, d, and s. The net sea contribution is further canceled by the cloud effect to bring the μ_n/μ_p ratio close to the experimental value. Barring any known symmetry principle yet to surface, this cancellation is probably accidental and in stark contrast with the $\pi N \sigma$ term and flavor-singlet g^0_A where the cloud and sea effects add up to enhance the SU(6) breaking [16].

The sea contribution from the u, d, and s quarks $G^{u,d}_{M,\mathrm{dis}}(q^2)$ and $G^s_M(q^2)$ are added to the valence and cloud part in the CI, $G_{M,\mathrm{con}}(q^2)$, to give the full $G^p_M(q^2)$ and $G^n_M(q^2)$. They are plotted in Figs. 4(a) and 4(b) and indicated by $\bullet$. Also plotted are the $G_{M,\mathrm{con}}(q^2)$ (denoted by $\bigcirc$) and the experimental fits (in solid line). We see from Fig. 4 and Table I that μ_p and μ_n are smaller than the experimental results by ~6% in absolute values. This is presumably due to the systematic errors of the finite volume, finite lattice spacing, and the quenched approximation. We should point out that in the earlier discussion of the μ_n/μ_p ratio, the systematic errors are expected to be cancelled out in the ratio to a large extent. Our conclusion of the ratio μ_n/μ_p in the preceding paragraph is thus based on this assumption.

A similar analysis is done for the strange Sachs electric form factor $G^s_E(q^2)$. This is plotted in Fig. 2(b). We see that
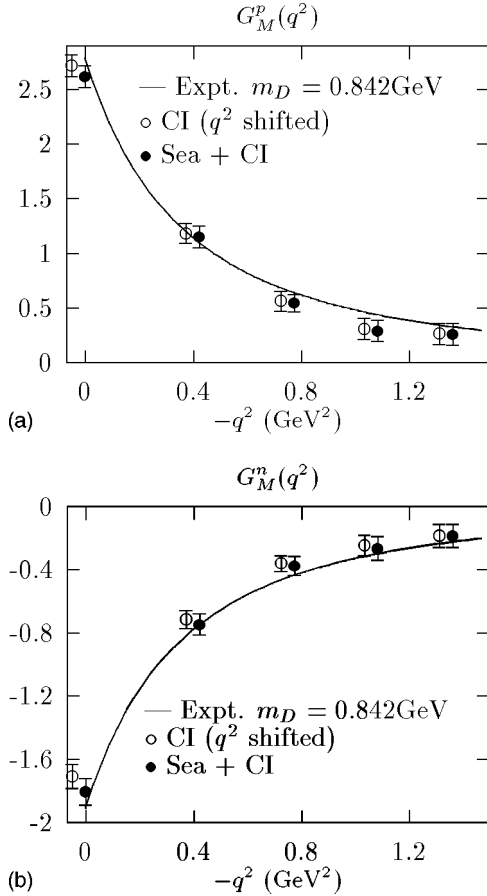
$$G^p_M(q^2)$$

(a)

$$G^n_M(q^2)$$

(b)

FIG. 4. (a) Proton magnetic form factor $G^p_M(q^2)$. The $\bigcirc$ from the CI are shifted to the left in $-q^2$ to avoid overlap with the full result (shown as $\bullet$). The solid line is the fit to the experiment [22]. (b) Neutron form factor $G^n_M(q^2)$.
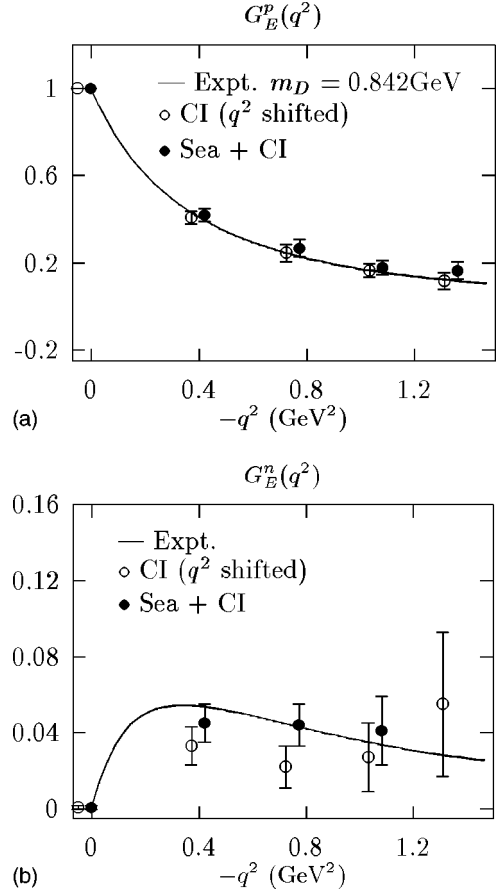
$$G^p_E(q^2)$$

(a)

$$G^n_E(q^2)$$

(b)

FIG. 5. (a) Proton electric form factor $G^p_E(q^2)$. (b) Neutron form factor $G^n_E(q^2)$.

$G_E^s(0)$ is consistent with zero as it should be. This serves as a test of the stochastic noise estimation. We fitted $G_E^s(q^2)$ with the form in Fig. 2(b) (solid line). This gives the electric mean-square radius $\langle r_s^2 \rangle_E = -0.061 \pm 0.003$ fm^2. In view of the large errors, we also plot the above form for $G_E^s(q^2)$ with m_M taken from $G_M^s(q^2)$ [shown as the dashed line in Fig. 2(b)]. This gives $\langle r_s^2 \rangle_E = -0.16 \pm 0.06$ fm^2 with $\chi^2 = 0.63$. This shows that that the uncertainty in the fitting can be as large as a factor of two. Nevertheless, $\langle r_s^2 \rangle_E$ is relatively small. This small negative value in $\langle r_s^2 \rangle_E$ and large negative $G_M^s(0)$ are consistent with the kaon loop picture [11] and VMD [12] but is inconsistent with most of the other model predictions [14].

Since the DI of u and d quarks are slighter larger than that of the s quark, the total sea contribution $G_{E,\mathrm{dis}}(q^2) = 2/3 G_{E,\mathrm{dis}}^u(q^2) - 1/3 G_{E,\mathrm{dis}}^d(q^2) - 1/3 G_E^s(q^2)$ adds a small positive value to the valence and cloud part $G_{E,\mathrm{con}}(q^2)$ in the CI. The proton $G_E^p(q^2)$ and neutron $G_E^n(q^2)$ are plotted in Figs. 5(a) and 5(b), respectively. We see that the CI part $G_{E,\mathrm{con}}^p(q^2)$ [shown as $\bigcirc$ in Fig. 5(a)] gives the main contribution in proton. $G_{E,\mathrm{dis}}(q^2)$ changes only a little. The resultant dipole fit gives a dipole mass of 0.857 ± 0.031 GeV. This is consistent with the experimental dipole mass of 0.842 GeV. In the case of the neutron, since $G_{E,\mathrm{con}}^n(q^2)$ itself ($\bigcirc$ in Fig. 5(b)] is small, the sea contribution $G_{E,\mathrm{dis}}(q^2)$ becomes a sizable part of the total $G_E^n(q^2)$ [$\bullet$ in Fig. 5(b)]. We see

that when the sea is included we have a reasonably good match with the experimental results [solid line in Fig. 5(b)]. The total mean square charge radius of -0.123 ± 0.019 fm^2 is obtained from fitting with the form which was used to fit the experimental results [22]. This is consistent with the experimentally fitted result of -0.127 fm^2.

In summary, we have calculated the s and u, d contributions to the electric and magnetic form factors of the nucleon. The individual MM and electric form factors from the different flavors in the sea are not small; however there are large cancellations among themselves due to the electric charges of the u, d, and s quarks. We find that a negative $G_M^s(0)$ leads to a total negative sea contribution to the nucleon MM which cancels the cloud effect to make the μ_n/μ_p ratio consistent with the experiment. We also find $G_E^s(q^2)$ positive and it leads to a postive total sea contribution to the neutron electric form factor $G_E^n(q^2)$. Future calculations are needed to investigate the systematic errors associated with the finite volume and lattice spacing as well as the quenched approximation.

[1] J. Ashman *et al.*, Nucl. Phys. **B328**, 1 (1989); B. Adeva *et al.*, Phys. Lett. B **329**, 399 (1994); K. Abe *et al.*, Phys. Rev. Lett. **74**, 346 (1995).

[2] J. Gasser, H. Leutwyler, and M. E. Sainio, Phys. Lett. B **253**, 252 (1991); **253**, 260 (1991).

[3] T. P. Cheng, Phys. Rev. D **13**, 2161 (1976); **38**, 2869 (1988).

[4] J. Gasser and H. Leutwyler, Phys. Rep. **87**, 77 (1982).

[5] SAMPLE Collaboration, B. Mueller *et al.*, Phys. Rev. Lett. **78**, 3824 (1997).

[6] D. B. Leinweber, Phys. Rev. D **53**, 5115 (1996).

[7] S. T. Hong, B. Y. Park, and D. P. Min, Phys. Lett. B **414**, 229 (1997).

[8] P. Geiger and N. Isgur, Phys. Rev. D **55**, 299 (1997).

[9] R. L. Jaffe, Phys. Lett. B **229**, 275 (1989).

[10] N. W. Park, J. Schechter, and H. Weigel, Phys. Rev. D **43**, 869 (1991).

[11] M. J. Musolf and M. Burkardt, Z. Phys. C **61**, 433 (1994).

[12] H. Forkel, M. Nielsen, X. Jin, and T. D. Cohen, Phys. Rev. C **50**, 3108 (1994).

[13] H.-W. Hammer, U.-G. Meissner, and D. Dreschel, Phys. Lett. B **367**, 323 (1996).

[14] C. V. Christov *et al.*, Prog. Part. Nucl. Phys. **37**, 1 (1996).

[15] Thomas Jefferson Lab proposals: No. PR-91-010, M. Finn and P. Souder, spokespersons; No. PR-91-017, D. Beck, spokesperson; and No. PR-91-004, E. Beise, spokesperson.

[16] S. J. Dong, J.-F. Lagaë, and K.-F. Liu, Phys. Rev. Lett. **75**, 2096 (1995); Phys. Rev. D **54**, 5496 (1996).

[17] M. Fukugita, Y. Kuramashi, M. Okawa, and A. Ukawa, Phys. Rev. Lett. **75**, 2092 (1995); Phys. Rev. D **51**, 5319 (1995).

[18] T. Draper, R. M. Woloshyn, and K. F. Liu, Phys. Lett. B **234**, 121 (1990); W. Wilcox, T. Draper, and K. F. Liu, Phys. Rev. D **46**, 1109 (1992).

[19] K. F. Liu, S. J. Dong, T. Draper, J. M. Wu, and W. Wilcox, Phys. Rev. D **49**, 4755 (1994); K. F. Liu, S. J. Dong, T. Draper, and W. Wilcox, Phys. Rev. Lett. **74**, 2172 (1995).

[20] S. J. Dong and K. F. Liu, Phys. Lett. B **328**, 130 (1994).

[21] J. Gasser, M. E. Sainio, and A. Švarc, Nucl. Phys. **B307**, 779 (1988).

[22] S. Galster *et al.*, Nucl. Phys. **B32**, 221 (1971).